

Aalborg Universitet



Electronically Reconfigurable Filtering Reflectarray Antenna Using Polarization Conversion Elements with Controllable Conversion Zeros

Fu, Wen; Cai, Yang; Mei, Peng; Pedersen, Gert Frølund; Zhang, Shuai

Published in:
I E E Transactions on Antennas and Propagation

DOI (link to publication from Publisher):
[10.1109/TAP.2024.3433577](https://doi.org/10.1109/TAP.2024.3433577)

Creative Commons License
Unspecified

Publication date:
2024

Document Version
Accepted author manuscript, peer reviewed version

[Link to publication from Aalborg University](#)

Citation for published version (APA):
Fu, W., Cai, Y., Mei, P., Pedersen, G. F., & Zhang, S. (2024). Electronically Reconfigurable Filtering Reflectarray Antenna Using Polarization Conversion Elements with Controllable Conversion Zeros. *I E E Transactions on Antennas and Propagation*, 72(9), 7359-7364. <https://doi.org/10.1109/TAP.2024.3433577>

General rights

Copyright and moral rights for the publications made accessible in the public portal are retained by the authors and/or other copyright owners and it is a condition of accessing publications that users recognise and abide by the legal requirements associated with these rights.

- Users may download and print one copy of any publication from the public portal for the purpose of private study or research.
- You may not further distribute the material or use it for any profit-making activity or commercial gain
- You may freely distribute the URL identifying the publication in the public portal -

Take down policy

If you believe that this document breaches copyright please contact us at vbn@aub.aau.dk providing details, and we will remove access to the work immediately and investigate your claim.

Electronically Reconfigurable Filtering Reflectarray Antenna Using Polarization Conversion Elements with Controllable Conversion Zeros

Wen Fu, *Graduate Student Member, IEEE*, Yang Cai, *Graduate Student Member, IEEE*, Peng Mei, *Member, IEEE*, Gert Frølund Pedersen, *Senior Member, IEEE*, and Shuai Zhang, *Senior Member, IEEE*

Abstract—This communication introduces an electronically reconfigurable filtering reflectarray antenna (RFRA) with good frequency selectivity and wide beam-scanning angle. The proposed reconfigurable element consists of a metal ring loading two PIN diodes at the ring openings, a patch with a complementary split ring, an E-shaped patch, a ground plate, and the DC biasing network for PIN diodes, which can not only convert the y -polarized incident wave into the x -polarized reflected wave, but also offer a 1-bit reflection phase. Furthermore, the proposed element can generate two controllable conversion zeros to permit high-selectivity filtering performance and adjustable bandwidth. A RFRA with 40×40 elements is analyzed in detail to demonstrate the filtering and beam-scanning capabilities, whose realized gain can reach 26.4 dBi at 29 GHz with an aperture efficiency (AE) of 15.7% and beam scanning angle can reach 60° . For lab-level verification, a 10×10 RFRA prototype has been fabricated and measured. The measurement and simulation results align well with each other, demonstrating that the proposed RFRA has good frequency selectivity and wide beam-scanning capabilities.

Index Terms—Filtering antenna, reflectarray, electronically reconfigurable, PIN diodes, polarization conversion, beam scanning.

I. INTRODUCTION

ANTENNAS are regarded as important components in wireless communication systems, receiving and transmitting electromagnetic waves. With the development of communication technologies, filtering antennas with both filtering response and radiation performance have been extensively investigated in the past few years. From the perspective of antenna design, the filtering antenna design methods are summarized into three different design methods in [1]. These three methods are essentially to generate radiation cancellation or radiation nulls, resulting in a good filtering response. With the increasing maturity of metasurface research, another filtering antenna design method has emerged based on reflectarray antennas (RAs) [2]–[5], [7]–[10] and transmitarray antennas (TAs) [11]–[19].

For RAs-based filtering antennas, the most critical step is to design a RA element with filtering response and phase shift capabilities simultaneously. In [2], a bandpass-like gain filtering RA was designed, whose element consists of a dielectric lens and a band-notched absorber to provide phase shift and filtering response, respectively. The gain versus frequency curve of the RA proposed in [3] shows sharp selectivity, which was achieved by integrating a filter with a substrate integrated waveguide (SIW) delay line. Using 3D printing technology, a unique filtering antenna design whose element consists of a two-section metal pixel waveguide was proposed in [4], which can achieve a filtering response with high selectivity by controlling the aperture amplitude and phase distributions at different frequencies. A 3-bit RA with a bandpass-like gain filtering property was designed in [5], whose element composed of a magnetoelectric (ME) dipole based on split ring resonators (SRRs) proposed in [6] and a phase delay line as the phase shifter can generate two

radiation nulls. Furthermore, some high-gain multifunctional filtering antennas have been proposed based on folded reflectarray antennas (FRAs) and frequency selective surfaces (FSSs) [7]–[10]. A FSS with quasi-elliptic bandpass response and polarization selectivity was proposed in [7] based on an antenna-filter-antenna (AFA) architecture, which was used as the sub-reflectarray of the FRA. By contrast, for TAs-based filtering antennas, there are generally two strategies to implement them. The most common strategy is the same as the RAs-based filtering antennas [11]–[17], and another one is to design a feed source with a filtering property [18] [19].

Although the previously-introduced filtering RAs and TAs can achieve high gain and good frequency selectivity, their elements are non-reconfigurable. In the design of reconfigurable elements, lumped components such as positive-intrinsic-negative (PIN) diodes [20]–[22], monolithic micro-electromechanical systems (MEMS) [23], varactor diodes [24], etc., and tunable materials like liquid crystals [25] [26], are widely used. However, previously reported RAs or TAs based on these reconfigurable elements do not have filtering functions. To the best of our knowledge, reconfigurable RAs or TAs with filtering characteristics have not been reported in the literature yet.

In this communication, a reconfigurable filtering RA (RFRA) with good frequency selectivity and wide beam-scanning angle is presented for the first time, whose element consists of a metal ring loading two PIN diodes at the ring openings, a patch with a complementary split ring, an E-shaped patch, a ground plate, and the DC-biasing network for PIN diodes. The proposed electronically RFRA element can offer a 1-bit reflection phase and generate two controllable conversion zeros to permit transmission zeros (TZs) for the RFRA. The proposed electronically RFRA can achieve beam scanning of 60° . As the scanning angle increases, the proposed electronically RFRA can still maintain good and stable filtering performance, which can be used in millimeter wave wireless systems to improve anti-interference capability and electromagnetic compatibility and achieve higher quality communications.

II. DESIGN OF 1-BIT ELECTRONICALLY RFRA ELEMENT

A. Structural Design of the 1-bit Electronically RFRA Element

In [27], a 180° phase difference was realized by controlling working states of the two PIN diodes placed in the mirror image, which was used to design a 1-bit electronically scanning transmitarray. Inspired by this, a 1-bit electronically RFRA element is proposed and its configuration is shown in Fig. 1. The element consists of three layers of substrate, five layers of metal, and two metalized vias. The three substrate layers are all Rogers RO4003C ($\epsilon_r = 3.55$), and the thicknesses are 0.508 mm, 0.305 mm, and 0.305 mm, respectively. They are glued together by Rogers RO4450F ($\epsilon_r = 3.52$) with a thickness of 0.2 mm. Fig. 1(b)–(d) sequentially presents the geometry of each metal layer. Here, the PIN diode with a model of MA4AGFCP910 from MACOM is adopted for the design. According to its data sheet [28], referring to the previous design using the same type of PIN diodes [29], the equivalent circuits of the PIN diode

Manuscript received xx x, 2024; revised xx x, 202x. (Corresponding author: Peng Mei.)

The authors are all with the Antennas, Propagation and Millimetre-Wave Systems (APMS) Section, Department of Electronic Systems, Aalborg University, Aalborg 9220, Denmark (e-mail: wf@es.aau.dk, wfu.ee@outlook.com; yangc@es.aau.dk; mei@es.aau.dk; gfp@es.aau.dk; sz@es.aau.dk).

operating at different modes are established as illustrated in Fig. 1(e). When the PIN diode is forward biased (state ON), it can be equivalent to a series circuit of a resistor of $R_{on} = 5.2 \Omega$ and an inductor of $L_{on} = 0.05 \text{ nH}$. By contrast, the PIN diode can be equivalent to a resistor of $R_{off} = 300 \text{ k}\Omega$ connected in parallel with a capacitor of $C_{off} = 21 \text{ fF}$ when it is reverse biased (state OFF). Copper layer 5 is the control circuit layer to excite PIN diodes, which is composed of DC bias line and fan-shaped stub. The fan-shaped stub is mainly to isolate DC signals and RF signals. The feeding via connects Copper layer 1 and Copper layer 5, while the shorting via connects Copper layer 1, Copper layer 2, Copper layer 3 and Copper layer 4. The detailed parameters of the proposed 1-bit electronically RFRA element are listed in Table I.

TABLE I
DIMENSIONS OF THE 1-BIT ELECTRONICALLY RFRA ELEMENT
(UNITS: mm)

Parameters	P	L_o	L_i	s_0	d_0	L_s	L_p
Values	3.85	3	2.2	0.3	0.2	1.2	3.5
Parameters	L_g	W_s	W_l	d_1	R_0	θ	
Values	2	0.2	3	0.6	0.6	90	

B. Full-wave Simulation and Performance Analysis

The proposed 1-bit electronically RFRA element is evaluated with CST Microwave Studio Suite. The boundary conditions in the X and Y directions are set to the unit cell, and the Z directions are set to Floquet ports. The element has two different working states. When the DC bias line and the feeding via are connected to a positive voltage (state 0), PIN 1 is forward-biased and PIN 2 is reverse-biased. By contrast, PIN 1 is reverse-biased and PIN 2 is forward-biased when the DC bias line and the feeding via are connected to a negative voltage (state 1). The simulated results of the element with two states under normal incidence are shown in Fig. 2. Fig. 2(a) shows the magnitudes of the reflection coefficients in two states are almost identical and the element can convert y -polarized incident wave into x -polarized reflected wave with a conversion loss of less than 1.3 dB. The phases of R_{xy} in two states always maintain a phase difference of 180° within the entire frequency range as shown in Fig. 2(b). The simulated results of the element under oblique incidence are shown in Fig. 3 taking the element working in state 0 as an example. It can be seen that the proposed element is quite oblique-incidence-insensitive. When the element is incident at a large angle, the reflection magnitude does not change much, and the phase has a certain deviation within an acceptable range.

To clarify the working principle that the proposed reconfigurable element can achieve two working states with a 180° reflection phase difference, the surface current of the element is studied and analyzed. As shown in Fig. 4, the surface currents of the Copper layer 1 along the x -direction are opposite in the two different states, indicating that the reflected x -polarized electromagnetic wave can produce a 180° reflection phase difference when the element is incident with a y -polarized electromagnetic wave in two working states [27].

C. Theoretical Analysis

To theoretically study the proposed polarization conversion element, a u - v coordinate system is defined by rotating the x - y coordinate system 45° . Assuming the normal incidence electromagnetic wave is y -polarized, it can be decomposed in the u - v coordinate system shown in the inset of Fig.5(a) and is expressed as

$$\vec{E}_i = \vec{E}_{iu} + \vec{E}_{iv} = \vec{u}E_{iu}e^{j\varphi} + \vec{v}E_{iv}e^{j\varphi} \quad (1)$$

where E_{iu} and E_{iv} represent the magnitudes of the incident electromagnetic wave and φ represent the phase of the incident

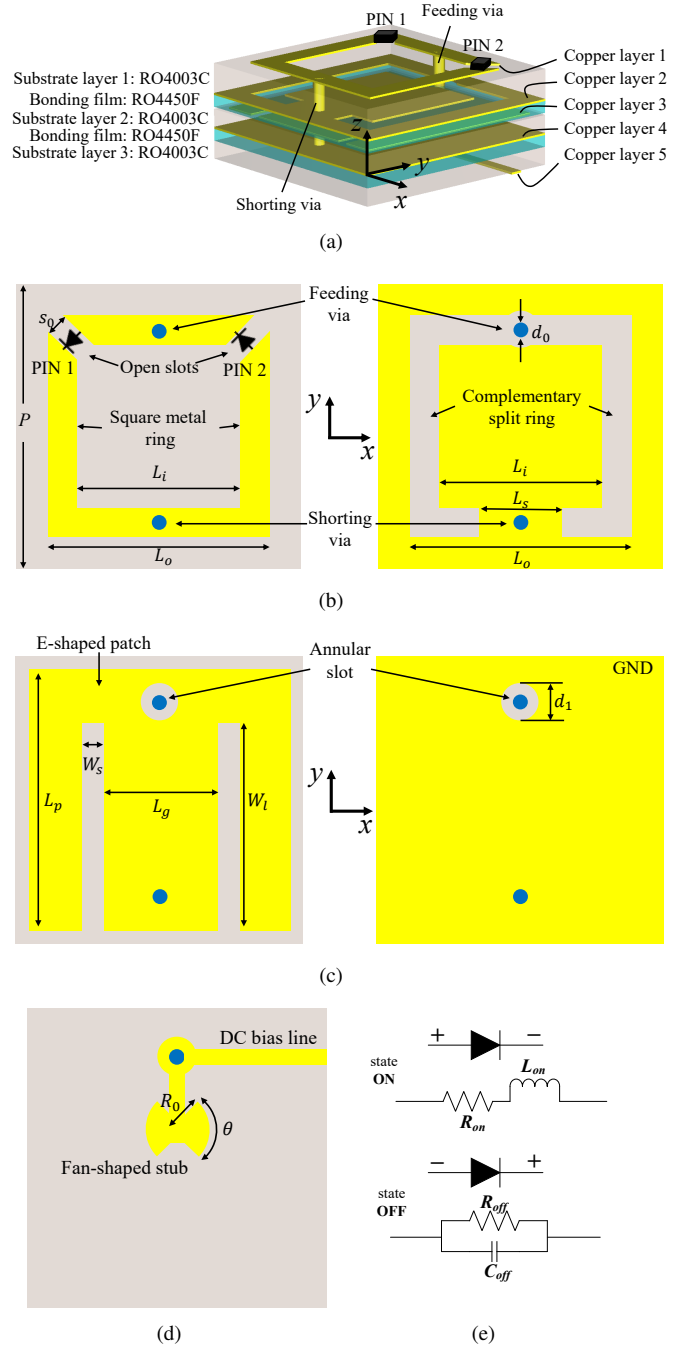


Fig. 1. Configuration of the proposed 1-bit electronically RFRA element. (a) 3D view. (b) The upper surface (Copper layer 1) and the lower surface (Copper layer 2) of the substrate layer 1. (c) The upper surface (Copper layer 3) and the lower surface (Copper layer 4) of the substrate layer 2. (d) The control circuit layer (Copper layer 5). (e) The equivalent circuit models of the PIN diode.

electromagnetic wave in the u - v coordinate system. The reflected electromagnetic wave in the u - v coordinate system can be expressed as

$$\vec{E}_r = \vec{E}_{ru} + \vec{E}_{rv} = \vec{u}r_{uu}E_{iu}e^{j(\varphi+\varphi_{uu})} + \vec{v}r_{vv}E_{iv}e^{j(\varphi+\varphi_{vv})} \quad (2)$$

where r_{uu} and r_{vv} are the reflection magnitudes and φ_{uu} and φ_{vv} are the reflection phases along the u - and v - directions.

If the magnitude difference $\Delta r_{uv} = |r_{uu} - r_{vv}| = 0$ and the phase difference $\Delta\varphi_{uv} = |\varphi_{uu} - \varphi_{vv}| = 180^\circ$, the 90° polarization conversion is perfectly realized, resulting in a reflected x -polarized electromagnetic wave. Within the frequency band (green region), the

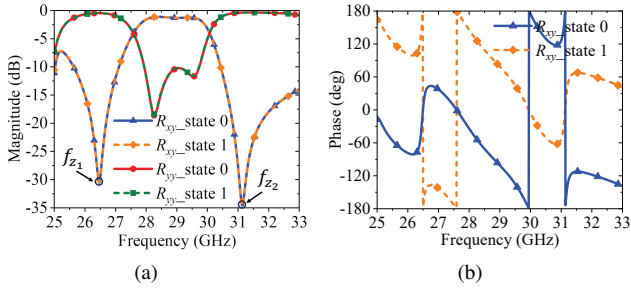


Fig. 2. Simulation results of the element under normal incidence for two states. (a) Magnitude. (b) Phase. (R_{xy} and R_{yy} are the reflection coefficients of x -polarization and y -polarization respectively when the polarization conversion element is illuminated by electromagnetic waves polarized in the y -direction.)

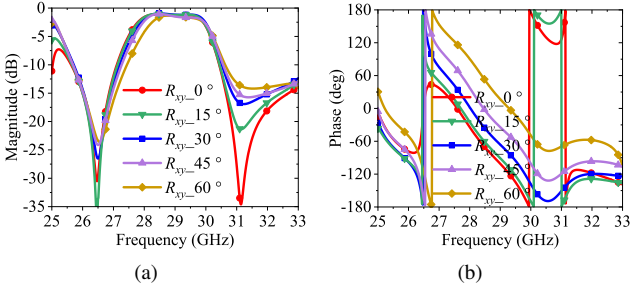


Fig. 3. Simulation results of the element with state 0 under oblique incidence. (a) Magnitude of R_{xy} . (b) Phase of R_{xy} .

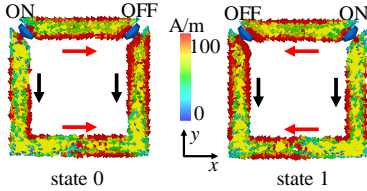


Fig. 4. Surface current on the Copper layer 1 of the element.

magnitude difference Δr_{uv} of r_{uu} and r_{vv} is small (less than 0.2) in Fig. 5(a), and the phase difference $\Delta\varphi_{uv}$ of φ_{uu} and φ_{vv} is $180^\circ \pm 45^\circ$ in Fig. 5(b), which satisfies the two conditions required for polarization conversion [30]–[32]. While there is no polarization conversion if $\Delta\varphi_{uv} = 0^\circ$, the two points where $\Delta\varphi_{uv} = 0^\circ$ in Fig. 5(b) are corresponding to two polarization conversion zeros in Fig. 2(a).

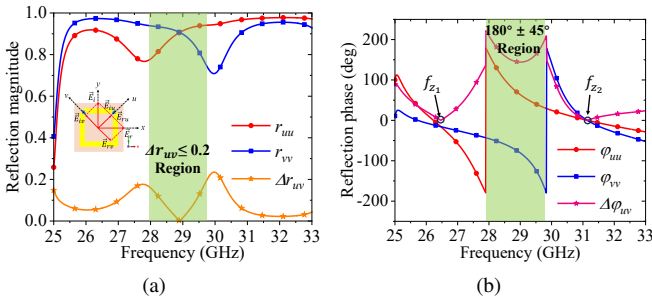


Fig. 5. Simulated reflection (a) magnitude and (b) phase under the u - v coordinate system.

D. Adjustable Conversion Zeros

Since the generation of the two conversion zeros ($f_{z1} = 26.5$ GHz and $f_{z2} = 31.2$ GHz) is the result of mutual coupling among the Copper layer 1, the Copper layer 2, and the Copper layer 3, the adjustments of parameters (i.e., L_i , L_o , L_s , L_p , W_l , W_s , L_g) can all manipulate the conversion zeros, which have been validated through full-wave simulations. Here, four representative manipulations of conversion zeros are presented in Fig. 6 by tuning specific

parameters. L_p can manipulate f_{z1} independently, while W_s controls f_{z2} independently. The bandwidth can be dynamically controlled with L_i . In addition, W_l is capable of tuning both conversion zeros simultaneously with a constant bandwidth.

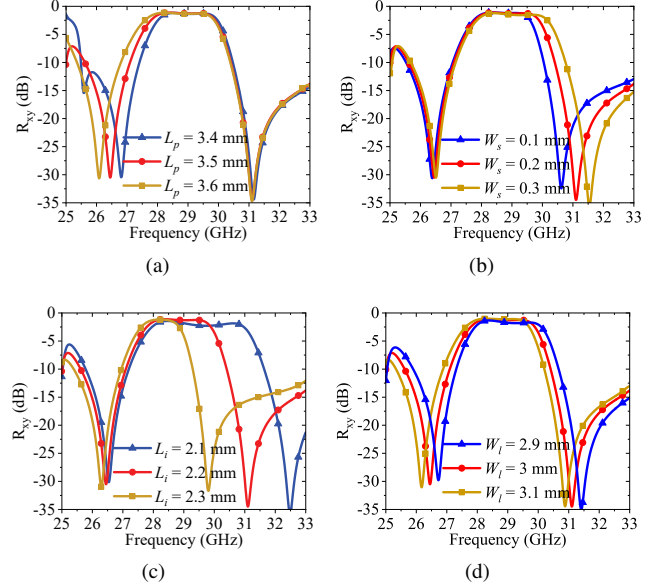


Fig. 6. Simulated R_{xy} when (a) L_p , (b) W_s , (c) L_i , and (d) W_l vary.

III. DESIGN OF 1-BIT ELECTRONICALLY RFRA

Based on the RFRA element proposed in Section II, a 1-bit electronically RFRA is presented, which is composed of 40×40 elements. A horn antenna with a model of PE9851B/2F-10 is adopted as the feed source operating from 22 GHz to 33 GHz, emitting y -polarized electromagnetic waves. According to [33], based on the comprehensive consideration for aperture efficiency (AE), the distance between the phase center of the feeding horn antenna and the geometrical center of the reflectarray aperture is set to 83 mm corresponding to the ratio of focal length to aperture diameter (F/D) is 0.54. In order to reduce the blockage as much as possible, the y -polarized horn antenna adopts an oblique incidence of 36° and points toward the geometrical center of the reflectarray aperture.

Fig. 7 shows the amplitude distribution, phase distribution with the main beam pointing to 0° . The edge taper (ET, the relative field strength at the edge of the reflectarray aperture with respect to the maximum) of reflectarray is at most -10 dB in Fig. 7(a), which is a typical and recommended value [34]. According to the phase calculation and quantization method in [35] [36], the continuous phase distribution and its corresponding 1-bit phase distribution are shown in Fig. 7(b) and Fig. 7(c). Ideally, the gain of the reflectarray using the phase distribution of Fig. 7(c) will theoretically be reduced by 4.89 dB compared with Fig. 7(b).

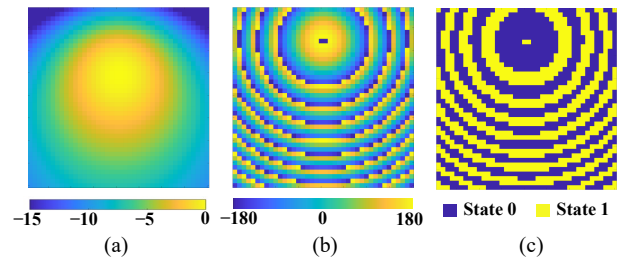


Fig. 7. (a) Amplitude distribution, (b) continuous phase distribution, and (c) 1-bit phase distribution of the reflectarray aperture.

To facilitate the beam scanning, the reflection phase of each element of the RFRA should be tunable, which can be achieved by altering the working states of the PIN diodes. Fig. 8 shows the radiation patterns when the main beam is scanned from 0° to 60° with a step of 15° in xoz -plane and yo -plane at 29 GHz. The maximum realized gain can reach 26.4 dBi at 29 GHz with an AE of 15.7%. As the beam-scanning angle increases, the realized gain decreases gradually, and the maximum realized gain decreases by 3.5 dB and 3.9 dB in xoz -plane and yo -plane, respectively. Fig. 9 shows the curves of realized gain versus frequency corresponding to different beam-scanning angles in xoz -plane and yo -plane. When the main beam is pointed at 0° , the realized gain curve shows a good frequency selectivity with two TZs that are mainly from the polarization conversion zeros of the RFRA element. With the increase of beam-scanning angle, the realized gain of the main beam of the RFRA decreases, but the filtering characteristic is always maintained. In addition, the simulation results show that as the beam-scanning angle changes, the cross-polarization level remains 15 dB lower than the principal polarization.

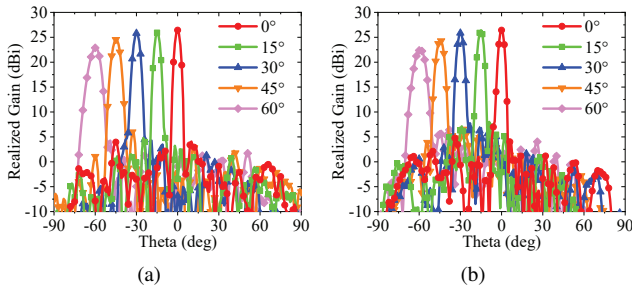


Fig. 8. Simulated radiation patterns for the main beam scanned from 0° to 60° with a step of 15° in (a) xoz -plane and (b) yo -plane at 29 GHz.

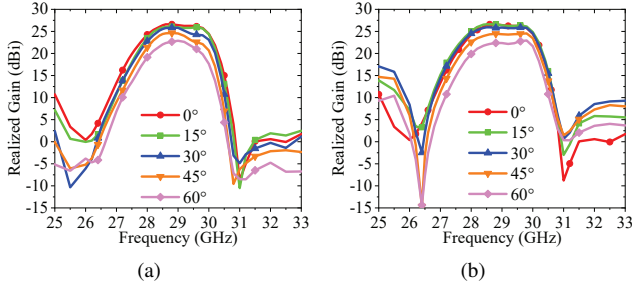


Fig. 9. Simulated realized gain corresponding to different beam scanning angles in (a) xoz -plane and (b) yo -plane.

In order to intuitively demonstrate the filtering capability of the proposed RFRA, the simulated radiation patterns of the broadside beam in xoz -plane and yo -plane at in-band center frequency and out-of-band TZs are given in Fig. 10. The maximum realized gain of the out-of-band TZ is at least 21 dB lower than the maximum realized gain of the in-band center frequency.

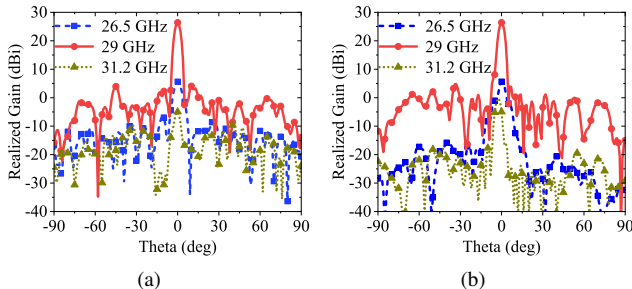


Fig. 10. Simulated radiation patterns of the broadside beam in (a) xoz -plane and (b) yo -plane at in-band center frequency and out-of-band TZs.

IV. EXPERIMENTAL VERIFICATION OF 1-BIT ELECTRONICALLY RFRA

A. Experimental Prototype

The 1-bit electronically RFRA with 40×40 elements proposed in Section III requires 3,200 PIN diodes, resulting in high laboratory costs for proof of concept. As a result, a prototype composed of 10×10 elements is fabricated for verification, which is a compromise between experimental performance and test costs.

The fabricated 1-bit electronically RFRA prototype and its experimental environment are shown in Fig. 11. The prototype adopts multi-layer printed circuit board (PCB) processing technology, with 200 PIN diodes welded on the uppermost layer. The PIN diodes of each element are connected to the DC bias line on the lowermost layer through metalized via. The other end of the DC bias line is connected to one pin of the flat flexible cable (FFC) connector. FFC jumper cables are used to connect the RFRA prototype and the control circuit adapter board. The control circuit adapter board with two FFC connectors and three insulation-displacement contact (IDC) socket connectors is designed for the connection between the power supply module and the RFRA prototype. The power supply module consists of three parts, field programmable gate array (FPGA), digital-to-analog converters (DAC), and direct current (DC) power supply. And it can be controlled by a personal computer (PC) to provide the required stable working voltage (± 2 V) for each element of the prototype. Fig. 12 gives a diagram of the control system for the fabricated RFRA prototype.

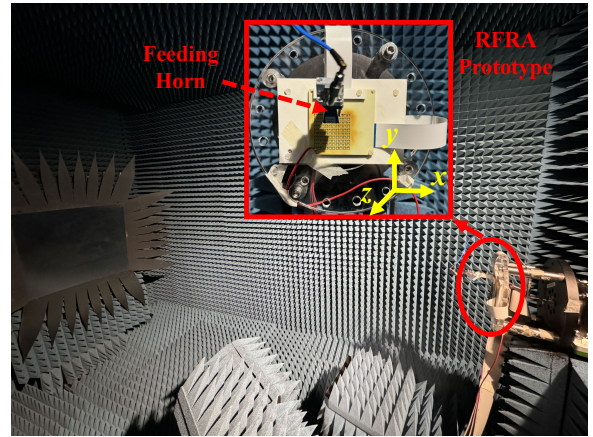


Fig. 11. Fabricated 1-bit electronically RFRA prototype and its experimental environment configuration.

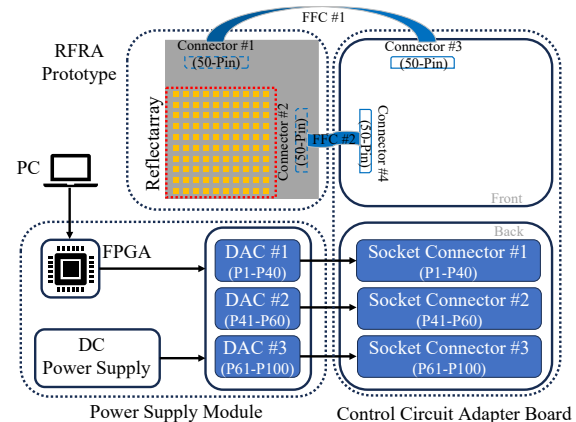


Fig. 12. Diagram of control system for the fabricated RFRA prototype.

TABLE II
COMPARISON OF THE PROPOSED RA WITH THE LATEST REPORTED RA

Ref.	Element configuration (Phase quantization)	Element No. (Array Size)	F/D	Freq. (GHz)	PRG (dBi)	AE (%)	Beam Scanning	Filtering characteristic	Selectivity
[5]	ME dipole + SRRs (3-bit)	52 * 52 (8.4λ ₀ * 8.4λ ₀)	0.64	10.5	24.3	30.56	No	Yes	~0.56
[7]	AFA-based FSS (patch with different slots) as sub-reflectarray (1-bit)	20 * 19 (9.1λ ₀ * 8.6λ ₀)	0.75	9.7	~20	10.22	No	Yes	~0.88
[20]	ME dipole + PIN diode (1-bit)	16 * 16 (6λ ₀ * 6λ ₀)	1.2	12.5	20.1	24	2D, 60°	No	No
[21]	Circular-slot + PIN diodes (1-bit)	16 * 16 (8λ ₀ * 8λ ₀)	1	73	16.8	6.2	2D, 70°	No	No
[22]	Segmented resonator with end folding + PIN diodes (2-bit)	36 * 36 (15.48λ ₀ * 15.48λ ₀)	0.87	26.1	29.2	27.1	2D, 50°	No	No
This Work	Patch loaded with slots + PIN diodes (1-bit)	40 * 40 (14.9λ ₀ * 14.9λ ₀)	0.54	29	26.4	15.7	2D, 60°	Yes	0.67
		10 * 10 (3.7λ ₀ * 3.7λ ₀)	0.68		11.9	8.9			0.64

* PRG: peak realized gain.

* λ₀ is the free-space wavelength corresponding to the working frequency of the antenna.

* Selectivity = $(f_{-3dB,U} - f_{-3dB,L}) / (f_{-10dB,U} - f_{-10dB,L})$, where -3(-10) dB denotes the gain level drop by 3(10) dB and U(L) denotes upper(lower) passband edge.

* In this work, the simulated results of reflectarray with 40*40 elements and the measured results of reflectarray with 10*10 elements are given in the comparison table.

B. Measurement Results

The 10 × 10 RFRA prototype uses the same feed source and feeding method as the 40 × 40 RFRA in Section III. The slight difference is that the distance between the phase center of the feeding horn antenna and the center of the reflectarray aperture of the prototype is 26 mm, resulting in a F/D of 0.68. Using the same method in Section III, the phase shift of each element of the RFRA prototype can be calculated, then 1-bit phase quantization is performed to obtain the element state distribution of the RFRA prototype. Accordingly, the beam scanning can be achieved by flexibly controlling the state ON or OFF of the PIN diodes on each element of the RFRA prototype using the control system shown in Fig. 12.

The simulated and measured radiation patterns of the RFRA prototype for the main beam scanned from 0° to 60° with a step of 15° in *xoz*-plane and *yo**z*-plane at 29 GHz are shown in Fig. 13. The measured maximum realized gain of the broadside beam at 29 GHz is 11.9 dBi with an AE of 8.9 %, compared to the simulated maximum realized gain of 12.6 dBi with an AE of 10.5%. When the beam is scanned to 60°, the measured maximum realized gain losses in *xoz*-plane and *yo**z*-plane are 3.2 dB and 3.3 dB, respectively. The simulated and measured realized gain corresponding to different beam scanning angles in *xoz*-plane and *yo**z*-plane are shown in Fig. 14. It can be seen that the curves of realized gain versus frequency corresponding to different beam scanning angles in *xoz*-plane and *yo**z*-plane exhibit a distinct filtering-like response with two TZs corresponding to two conversion zeros introduced by the proposed RFRA element, which shows the RFRA prototype has good filtering characteristic and frequency selectivity.

Comparing the measured and simulated results, the discrepancy is generally acceptable taking into account actual fabrication errors, assembling errors, and imperfect soldering of PIN diodes. The errors caused by the processing accuracy and assembling of multi-layer PCB are the main reasons for the filtering frequency bandwidth shifts in Fig. 14, which can be proved in Fig. 6. The reduction of realized gain and the deviation of scanning angles in Fig. 13

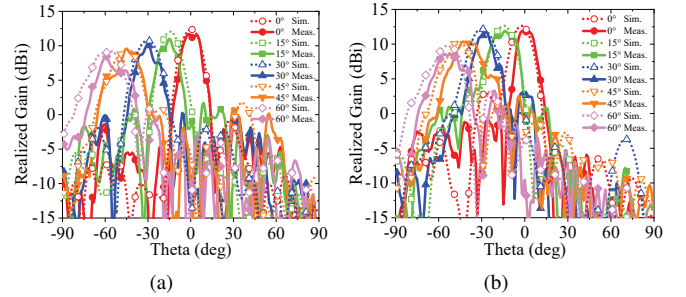


Fig. 13. Simulated and measured radiation patterns for the main beam scanned from 0° to 60° with a step of 15° in (a) *xoz*-plane and (b) *yo**z*-plane at 29 GHz.

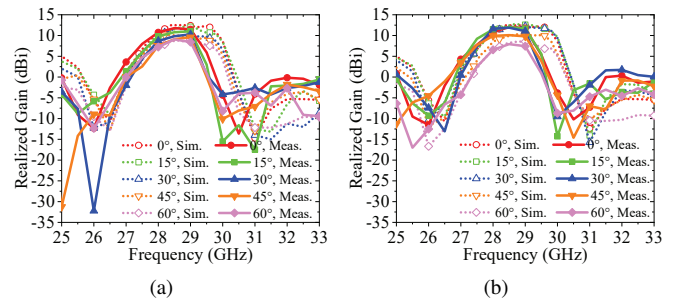


Fig. 14. Simulated and measured realized gain corresponding to different beam scanning angles in (a) *xoz*-plane and (b) *yo**z*-plane.

are caused by the phase errors. The phase errors are introduced due to the imperfect soldering of PIN diodes resulting in poor consistency of elements on the array and causing the equivalent circuit parameters of PIN diodes inconsistent with simulation settings [20] [37]. More importantly, since the feed source illuminates the reflectarray obliquely, the specular reflection would lead to reduced gain and worse sidelobe levels (SLLs) [38].

C. Comparison

The RFRA proposed in this communication is compared with the latest reported RAs in Table II. Compared with [5] and [7], the selectivity of the proposed RFRA is at a medium level, but it can achieve wide-angle beam scanning. The selectivity of the filtering antenna here is calculated based on the broadside beam. The closer the calculated result is to 1, the better the selectivity of the filtering antenna is. Compared with [20]–[22], although they can both achieve beam scanning, they do not have filtering functions. The RFRA proposed in this communication can not only achieve wide beam-scanning angle, but also feature good filtering characteristics, which is presented for the first time.

V. CONCLUSION

An electronically RFRA with good frequency selectivity and large-angle beam-scanning capabilities is presented, whose elements can perform multiple functions: polarization conversion, 1-bit phase shift, and providing TZs. A RFRA with 40×40 elements is analyzed in detail. A 10×10 RFRA prototype is fabricated and measured for proof of concept. The measured and simulated results align well with each other, demonstrating that the proposed RFRA has good frequency selectivity and large-angle beam-scanning capabilities. It not only meets the multi-functional requirements of antenna design, but also improves anti-interference capability and electromagnetic compatibility, which can be used in millimeter wave wireless systems to achieve higher quality communications.

REFERENCES

- [1] S. S. Ji, Y. D. Dong, and Y. Fan, "Bandpass Filter Prototype Inspired Filtering Patch Antenna/Array," *IEEE Trans. Antennas Propag.*, vol. 70, no. 5, pp. 3297-3307, May 2022.
- [2] P. Mei *et al.*, "A Reflectarray Antenna Designed With Gain Filtering and Low-RCS Properties," *IEEE Trans. Antennas Propag.*, vol. 67, no. 8, pp. 5362-5371, Aug. 2019.
- [3] J. Zhang *et al.*, "Analysis and Design of Reflectarray Antennas Based on Delay Lines: A Filter Perspective," *IEEE Access*, vol. 8, pp. 44947-44956, 2020.
- [4] G. B. Wu *et al.*, "High-Gain Filtering Reflectarray Antenna for Millimeter-Wave Applications," *IEEE Trans. Antennas Propag.*, vol. 68, no. 2, pp. 805-812, Feb. 2020.
- [5] Z. Y. Xu *et al.*, "A Highly Selective Reflectarray Using ME Dipole Element with Gain Filtering Characteristic," *IEEE Trans. Antennas Propag.*, vol. 72, no. 2, pp. 1989-1994, Feb. 2024.
- [6] H. W. Lin *et al.*, "High-Selectivity FA-FA-Based Frequency Selective Surfaces Using Magneto-electronic Dipole Antennas," *IEEE Trans. Antennas Propag.*, vol. 70, no. 11, pp. 10669-10677, Nov. 2022.
- [7] M. Jiang *et al.*, "Frequency Selective Surface with Quasi-Elliptic Bandpass Response for Filtering FRA Application," *IEEE Trans. Antennas Propag.*, vol. 72, no. 1, pp. 1004-1008, Jan. 2024.
- [8] X. C. Zhu *et al.*, "A High-Gain Filtering Antenna Based on Folded Reflectarray Antenna and Polarization-Sensitive Frequency Selective Surface," *IEEE Antennas Wireless Propag. Lett.*, vol. 19, no. 8, pp. 1462-1465, Aug. 2020.
- [9] Z. M. Du *et al.*, "Multifunctional Folded Reflectarray Antenna for Circular Polarization and High-Gain Filtering," in *Proc. iWEM*, Guangzhou, China, 2021.
- [10] P. P. Zhang *et al.*, "Design of Filtering Folded Reflectarray Antenna Through Exploiting Its Main Reflectarray," in *Proc. IMWS-AMP*, Guangzhou, China, 2022.
- [11] P. Mei *et al.*, "A Millimeter-Wave Gain-Filtering Transmitarray Antenna Design Using a Hybrid Lens," *IEEE Antennas Wireless Propag. Lett.*, vol. 18, no. 7, pp. 1362-1366, July 2019.
- [12] L. Wen *et al.*, "Wideband Transmitarray Antenna Using Compact 2-bit Filtering Unit Cells," *IEEE Trans. Antennas Propag.*, vol. 71, no. 10, pp. 8344-8349, Oct. 2023.
- [13] T. Hu *et al.*, "An Ultrathin Transmitarray Antenna With High Frequency Selectivity Using Antenna-Filter-Antenna Structure," *IEEE Antennas Wireless Propag. Lett.*, vol. 22, no. 12, pp. 3072-3076, Dec. 2023.
- [14] Q. S. Jia *et al.*, "A Broadband Filtering Circularly Polarized Folded Transmitarray Antenna Based on Metasurface," *IEEE Antennas Wireless Propag. Lett.*, vol. 22, no. 10, pp. 2357-2361, Oct. 2023.
- [15] P. Y. Feng, S. W. Qu, and S. W. Yang, "Dual-Polarized Filtering Transmitarray Antennas With Low-Scattering Characteristic," *IEEE Trans. Antennas Propag.*, vol. 69, no. 11, pp. 7965-7970, Nov. 2021.
- [16] P. Y. Feng *et al.*, "Integrative Transmitarray With Gain-Filtering and Low-Scattering Characteristics," *IEEE Trans. Antennas Propag.*, vol. 70, no. 3, pp. 1931-1939, Mar. 2022.
- [17] Y. Cao *et al.*, "Cavity-Filter-Based 3-D-Printed Gain-Filtering Transmitarray for Multibeam Applications," *IEEE Trans. Antennas Propag.*, vol. 71, no. 12, pp. 9685-9695, Dec. 2023.
- [18] H. T. Hu *et al.*, "V-Band Dual-Polarized Filtering Transmitarray Antenna Enabled by a Planar Filtering Illumination Source," *IEEE Trans. Antennas Propag.*, vol. 70, no. 10, pp. 9184-9197, Oct. 2022.
- [19] H. T. Hu, K. F. Chan, and C. H. Chan, "Low-Profile Circular-Polarized Filtering Transmitarray Antenna in V-Band," *IEEE Trans. Antennas Propag.*, vol. 72, no. 1, pp. 938-943, Jan. 2024.
- [20] B. J. Xiang, X. Dai, and K. M. Luk, "A Wideband Low-Cost Reconfigurable Reflectarray Antenna With 1-Bit Resolution," *IEEE Trans. Antennas Propag.*, vol. 70, no. 9, pp. 7439-7447, Sept. 2022.
- [21] C. Liu *et al.*, "An E-Band Reconfigurable Reflectarray Antenna Using p-i-n Diodes for Millimeter-Wave Communications," *IEEE Trans. Antennas Propag.*, vol. 71, no. 8, pp. 6924-6929, Aug. 2023.
- [22] E. Wang *et al.*, "A 1296-Cell Reconfigurable Reflect-Array Antenna With 2-bit Phase Resolution for Ka-Band Applications," *IEEE Trans. Antennas Propag.*, vol. 72, no. 4, pp. 3425-3437, April 2024.
- [23] T. Debogetic and J. Perruisseau-Carrier, "Low Loss MEMS-Reconfigurable 1-Bit Reflectarray Cell With Dual-Linear Polarization," *IEEE Trans. Antennas Propag.*, vol. 62, no. 10, pp. 5055-5060, Oct. 2014.
- [24] S. Costanzo *et al.*, "Dual-Layer Single-Varactor Driven Reflectarray Cell for Broad-Band Beam-Steering and Frequency Tunable Applications," *IEEE Access*, vol. 6, pp. 71793-71800, 2018.
- [25] P. Aghabeyki *et al.*, "Optically Transparent Beam-Steering Reflectarray Antennas Based on a Liquid Crystal for Millimeter-Wave Applications," *IEEE Trans. Antennas Propag.*, vol. 72, no. 1, pp. 614-627, Jan. 2024.
- [26] X. Li *et al.*, "Development of Two-Dimensional Steerable Reflectarray With Liquid Crystal for Reconfigurable Intelligent Surface Applications," *IEEE Trans. Antennas Propag.*, vol. 72, no. 3, pp. 2108-2123, March 2024.
- [27] H. Yu *et al.*, "A Novel Wideband and High-Efficiency Electronically Scanning Transmitarray Using Transmission Metasurface Polarizer," *IEEE Trans. Antennas Propag.*, vol. 70, no. 4, pp. 3088-3093, Apr. 2022.
- [28] MACOM Company. MA4AGFCP910 Aluminum Gallium Arsenide Flip Chip PIN Diode. Accessed on: 2023. [Online]. Available: https://cdn.macom.com/datasheets/MA4AGP907_MA4AGFCP910.pdf
- [29] J. Zhang *et al.*, "Radiation-Pattern Reconfigurable Phased Array With p-i-n Diodes Controlled for 5G Mobile Terminals," *IEEE Trans. Microw. Theory Tech.*, vol. 68, no. 3, pp. 1103-1117, Mar. 2020.
- [30] X. Huang *et al.*, "Ultrathin Dual-Band Metasurface Polarization Converter," *IEEE Trans. Antennas Propag.*, vol. 67, no. 7, pp. 4636-4641, July 2019.
- [31] C. Fu *et al.*, "Dual-Bandwidth Linear Polarization Converter Based on Anisotropic Metasurface," *IEEE Photon. J.*, vol. 12, no. 2, pp. 1-11, Apr. 2020.
- [32] S. Pramanik *et al.*, "Active Metasurface-Based Wideband Polarization Converter With a Switchable Notch," *IEEE Trans. Electromagn. Compat.*, vol. 65, no. 4, pp. 1081-1089, Aug. 2023.
- [33] A. Yu *et al.*, "Aperture efficiency analysis of reflectarray antennas," *Microw. Opt. Technol. Lett.*, vol. 52, no. 2, pp. 364-372, Feb. 2010.
- [34] P. Nayeri, F. Yang, and A. Z. Elsherbeni, *Reflectarray Antennas: Theory, Designs, and Applications*. Hoboken, NJ, USA: Wiley, 2018.
- [35] P. Mei, S. Zhang, and G. F. Pedersen, "A Low-Cost, High-Efficiency and Full-Metal Reflectarray Antenna With Mechanically 2-D Beam-Steerable Capabilities for 5G Applications," *IEEE Trans. Antennas Propag.*, vol. 68, no. 10, pp. 6997-7006, Oct. 2020.
- [36] S. G. Zhou *et al.*, "A Wideband 1-Bit Reconfigurable Reflectarray Antenna at Ku-Band," *IEEE Antennas Wireless Propag. Lett.*, vol. 21, no. 3, pp. 566-570, March 2022.
- [37] X. Dai, G. B. Wu, and K. M. Luk, "A Wideband Low-Profile Reconfigurable Transmitarray Using Magneto-electric Dipole Elements," *IEEE Trans. Antennas Propag.*, vol. 70, no. 9, pp. 8008-8019, Sept. 2022.
- [38] H. Yang *et al.*, "A 1-Bit 10×10 Reconfigurable Reflectarray Antenna: Design, Optimization, and Experiment," *IEEE Trans. Antennas Propag.*, vol. 64, no. 6, pp. 2246-2254, June 2016.